Human Factors in Design, Engineering, and Computing, Vol. 238, 2026, 2917–2926
https://doi.org/10.54941/ahfe1008515

Fabric-Based Wearable Sensors for Multimodal Motion and Pressure Tracking

Ganit Goldstein, Amit Schechter, Skylar Tibbits, and Dava Newman

Massachusetts Institute of Technology, Cambridge, MA 02139, USA

ABSTRACT

We present a pilot study of a customized wearable sleeve prototype with sensing elements for the assessment of multimodal motion and pressure tracking with activity classification. The system combines APDM OPAL inertial measurement units (IMUs), textile-embedded flexible pressure-sensing matrices, and a video camera used as an external kinematic reference. The pressure sensors capture localized variations in body–garment interaction during movement, while the IMUs provide complementary measurements of joint motion and segment orientation. Integrating these sensing modalities enables the characterization of movement patterns, pressure distributions, and their relationship to different activities. The proposed framework offers a portable and human-centered approach for multimodal wearable sensing, with potential applications in ergonomics, smart garments, rehabilitation, and activity monitoring.

Keywords: Wearable sensing, Smart textiles, Activity classification, Motion tracking, Pressure sensing, Multimodal sensing

INTRODUCTION

Wearable technologies have increasingly been used in the study of human movement, enabling continuous monitoring across a range of applications. Common approaches include inertial measurement units (IMUs), motion-tracking systems, and physiological sensing modalities such as sEMG, cardiorespiratory, thermal, and sweat sensing (Iosa et al., 2016; Porciuncula et al., 2018; Angelucci et al., 2021; Homayounfar and Andrew, 2020). Smart textiles extend wearable technologies by embedding sensing elements directly into fabrics and garments, enabling the measurement of mechanical responses such as pressure and strain while maintaining the flexibility and conformability of textiles (Abouraddy et al., 2007; Castano and Flatau, 2014; Stoppa and Chiolerio, 2014; Zhang et al., 2022).

These sensing technologies can characterize human movement through different forms of data and representation, including kinematic measurements, motion patterns, skeletal representations, and pressure distributions (Moeslund et al., 2006; Iosa et al., 2016; Cheng et al., 2016). However, these technologies often focus on individual aspects of human movement, and their outputs are frequently analyzed independently, making it difficult to directly relate body motion to the corresponding mechanical response within the body–garment interface. In particular, changes in body position and joint motion can produce localized variations in garment pressure,

Received September 25, 2026; Revised October 27, 2026; Accepted November 7, 2026; Available online December 1, 2026

© 2026 The Authors. This work is licensed under a Creative Commons Attribution-NonCommercial-NoDerivatives 4.0 License.
For more information, see https://creativecommons.org/licenses/by-nc-nd/4.0/

creating patterns that may provide additional information about the activity being performed (Xu et al., 2022; Piao et al., 2023). A multimodal sensing approach can help address this relationship by synchronizing and integrating complementary sensing modalities within a common framework. Combining information from multiple sensor types can provide a more comprehensive representation of human activity and may support more direct investigation of the relationship between dynamic body motion and garment–body mechanical interactions (Gravina et al., 2017; Mokhlespour Esfahani and Nussbaum, 2019; Qiu et al., 2022).

In this work, we investigate this approach through a custom-fitted sleeve based on body scan, with IMUs, pressure-sensing matrices, and a video camera as an external kinematic reference. By comparing individual and combined sensing modalities, this work explores how multimodal information can support activity classification and inform the integration of multiple sensing technologies into wearable garments.

DEVELOPING MULTIMODAL WEARABLE SYSTEM

The sleeve prototype sensing system was developed to capture complementary aspects of upper-limb movement by integrating pressure sensors at the elbow and palm, together with two APDM OPAL inertial measurement units (IMUs) positioned at the upper arm and wrist. The pressure sensors were LOOMIA Mini Matrix FSRs, flexible force-sensitive resistor arrays consisting of nine 8.9 mm sensing cells arranged in a 3 × 3 matrix within an approximately 46 × 53 mm area. The participant's 3D body-scan geometry was converted into a two-dimensional sleeve pattern using Rhino and CLO 3D, enabling the scanned surface to be translated into a custom-fitted garment pattern. The sleeve was then fabricated using digital embroidery and divided into six sections. An Intel RealSense D435i camera was positioned in front of the participant to provide an external visual reference for movement. Although the device is a depth camera, the camera-based analysis in this study used 2D pose estimates extracted from the RGB image stream rather than depth-derived 3D skeletal measurements. IMU, pressure, and camera data were acquired with corresponding timestamps and aligned within a common synchronization and computational framework.

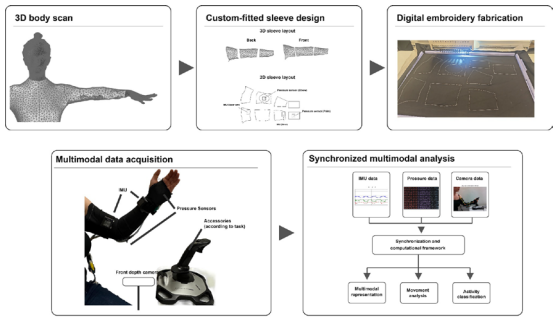


Figure 1: Overview of the workflow, including 3D body scanning, custom-fitted sleeve design, digital embroidery fabrication, multimodal data acquisition using IMU, pressure, and depth camera, followed by synchronized multimodal analysis for movement and activity assessment.

EXPERIMENTAL PROTOCOL AND DATA COLLECTION

A single participant wore the customized sleeve, designed from the participant's 3D body scan, with pressure-sensing matrices positioned at the elbow and hand and APDM OPAL IMUs attached to the upper arm and wrist (Figure 2a). Four activities were selected to represent functional, resistance, and coordination-based movements: drinking, weight lifting, resistance-band stretching, and joystick play (Figure 2b–e). The participant performed 10 consecutive repetitions of each activity in a single recording session, while the sleeve and sensor placement remained unchanged.

Pressure-sensing matrices were integrated at the elbow and palm to capture contact changes during movement and connected to custom electronics via an Arduino Leonardo. Custom scripts developed in the Arduino IDE and Visual Studio Code were used to acquire and process signals from pressure-sensing matrices at the hand and elbow. The signals were baseline-corrected, filtered, and recorded as processed ADC counts (arbitrary units), representing relative changes in contact pressure. IMU data were recorded from the upper arm and wrist using Motion Studio software at 128 Hz, pressure data at approximately 15 Hz (median 14.7 Hz), and video at 30 fps with a resolution of 640 × 480 pixels. All data streams were timestamped using the recording computer clock and temporally aligned using the three-clap synchronization event, with an estimated alignment accuracy of approximately 0.1 s.

For a separate range-of-motion experiment, the participant completed four additional resistance-band stretching trials using the same sensor configuration. The instructed conditions included full range of motion, approximately 80% and 50% of full range, and a trial transitioning from full range to approximately 50% range during the recording. These trials were used to evaluate whether the multimodal sleeve signals could differentiate between instructed ranges of motion.

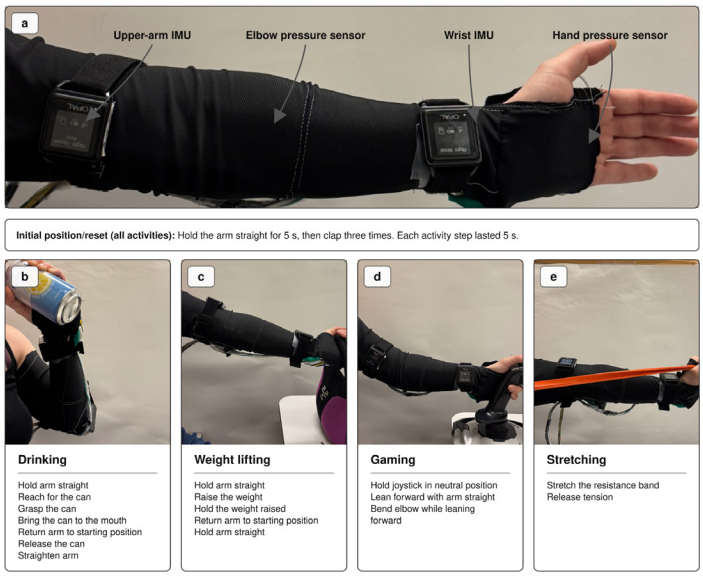


Figure 2: System and protocol. Sleeve and sensor placement (a) with four task images, including drinking (b), weight lifting (c) joystick play (d) and stretching a resistance band (e).

COMPUTATIONAL EXPERIMENTS

The computational pipeline synchronized the IMU, pressure, and video recordings, extracted movement and contact signals, compared the IMU motion estimate with video-based pose estimation, and evaluated classification of activity and stretching range of motion.

Data Preprocessing and Synchronization

Two IMUs, pressure sensors, and a video camera recorded data using a shared computer clock timestamp. At the start of a session, the participant held a neutral arm position for five seconds and clapped three times. Acceleration peaks from the claps defined the start of the recording; corresponding events in the video and pressure signals confirmed multimodal alignment within approximately 0.1 seconds. IMU signals were low-pass filtered at 10 Hz, and IMU and pressure data were linearly interpolated onto a common 30 Hz timeline. Elbow motion was calculated from the wrist IMU's orientation relative to the upper-arm IMU, referenced to the neutral pose. Gyroscope magnitude described movement speed, acceleration variation described impacts, and mean acceleration along each axis described static posture. An IMU-kinematic feature set was defined to isolate movement dynamics from static posture, combining the elbow angle, gyroscope magnitude, and acceleration variation while excluding mean acceleration. We identified active movement from the gyroscope signal and segmented repetitions from the smoothed elbow-angle trace, with visual verification. For each repetition, we calculated duration, angle range, movement speed, and hand and elbow sensor responses. To compare repetitions of different lengths, we mapped each one to 0-100% of its duration and summarized the traces across repetitions (Figure 3).

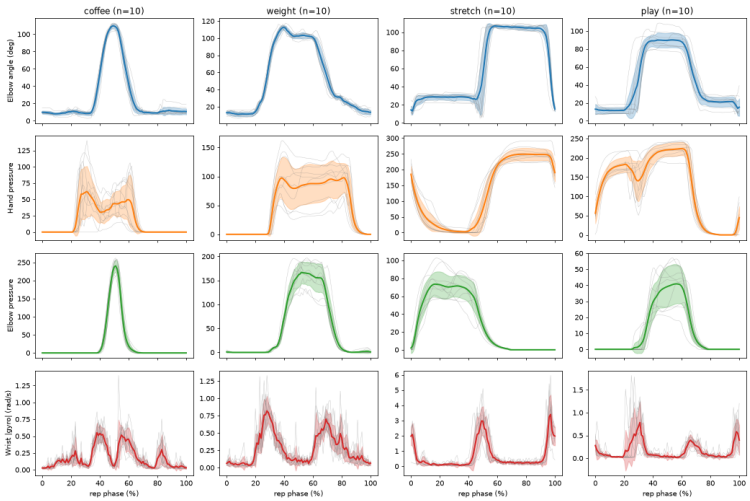


Figure 3: Motion and sensor responses during drinking, weight lifting, stretching, and joystick play (10 repetitions each). Each repetition is mapped to a common normalized phase from start to finish. Rows show elbow angle, hand pressure response, elbow pressure response, and wrist gyroscope magnitude.

Video-Based Motion Comparison

We used RT-DETR (Zhao et al., 2024) to locate the participant and ViTPose to identify the shoulder, elbow, and wrist in each video frame. These markers defined a two-dimensional elbow angle. Frames without adequate joint detection or camera coverage were excluded (any of the three joints below 0.5 confidence, or the elbow/wrist outside the frame; short gaps of ≤15 frames were interpolated). This excluded 3.9% of frames for stretching and 0.6% for joystick play overall, with essentially no exclusion during the repetitions actually compared (coverage was ~100% within the active/raised phase of each rep for both activities). The weight-lifting recording was excluded because the arm was not tracked reliably. The camera angle and IMU angle represent different geometric measurements, so we linearly rescaled the camera trace to the IMU trace by least squares before comparing their timing and shape. We assessed agreement using correlation and counted repetitions independently in the video and IMU traces (Figure 4).

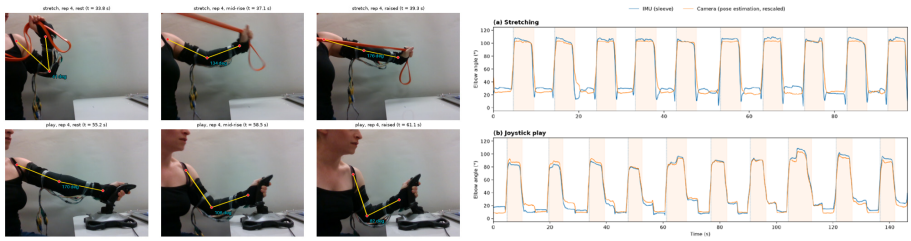


Figure 4: Comparison of IMU-derived and camera-derived elbow motion. Left: Video frames from stretching (top) and joystick play (bottom), with detected shoulder, elbow, and wrist positions (yellow) and the two-dimensional elbow angle. Right: Elbow-angle traces across 10 repetitions of stretching (a) and joystick play (b). Blue shows the relative orientation of the wrist and upper-arm IMUs; orange shows the camera-derived angle, linearly rescaled to the IMU trace. Shading marks movement phases detected from video; dotted lines mark repetition onsets detected from the IMUs.

Activity Classification

We classified the four activities using L2-regularized (Krogh and Hertz, 1991), logistic regression (McCullagh and Nelder, 1989) and a 300-tree random forest (Breiman, 2001). Models used either complete repetitions or three-second windows, drawn from each recording's active period. Features summarized elbow motion, IMU movement and posture signals, and hand and elbow sensor responses. We compared IMU features, pressure features, their combination, and restricted feature sets to assess the contribution of each signal. We evaluated the models using blocked temporal cross-validation. Each recording was divided into four contiguous blocks; in each fold, one block from every activity was held out, and nearby training samples were removed with a guard interval. Activities were recorded in a single session. The resulting accuracies describe separation of these recordings and should be further tested to conclude performance on new participants or sessions.

Range-of-Motion Classification

To examine whether measurements from the sleeve could distinguish movements within a single activity, we used the range-of-motion stretching recordings which were designed to capture movements in various ranges of motion. We applied the same segmentation, feature extraction, blocked cross-validation, and sensor comparisons used for activity classification. Models classified either the four recording conditions or full range versus the other three conditions combined, using complete repetitions (n = 40) or three-second windows.

RESULTS AND DISCUSSION

Motion and Pressure Responses Across Activities

The sleeve produced usable IMU and pressure recordings for all 40 repetitions of the four activities. After aligning repetitions by movement phase, the recorded activities showed different combinations of elbow motion, movement speed, and hand and elbow sensor responses. Drinking produced a brief elbow-sensor response near maximum flexion, whereas stretching and joystick play produced more sustained hand-sensor responses. Weight lifting produced responses at both sensor locations. The pressure signals also differed between activities at similar estimated elbow angles. Near 100° during flexion, the median hand-sensor response was approximately 29 counts for drinking and 170 counts for joystick play; the corresponding elbow-sensor responses were approximately 51 and 20 counts. Thus, elbow angle alone did not describe all of the differences observed in the textile sensors.

Comparison With Camera-Derived Motion

For stretching and joystick play, the camera-derived and IMU-derived elbow-angle traces showed similar movement timing and repetition patterns (Figure 4). The video analysis identified the same repetitions as the IMU analysis. Elbow-angle traces were strongly correlated after this rescaling (Pearson r = 0.97 for stretching and r = 0.99 for joystick play; RMSE = 10.0° and 4.8°, respectively). Weight lifting could not be included because the arm was not tracked reliably in the video. The camera measured a two-dimensional projected angle, whereas the IMUs measured relative sensor orientation. The camera trace was therefore linearly rescaled before the comparison. This result supports consistency in the timing and shape of the two motion estimates; it does not establish the absolute accuracy of the IMU-derived elbow angle.

Classification of the Recorded Activities

Within this participant's recordings, the four activities were distinguishable from the wearable signals (Table 1). Using complete repetitions, combined IMU and pressure features and pressure features alone each achieved 100% accuracy under blocked temporal cross-validation. For three-second windows, combined features achieved 99% accuracy, while pressure

features alone achieved 79%. The shorter windows therefore contained less of the activity-specific pressure pattern than complete repetitions did, and in this setting multimodal input provided performance improvement. Adding pressure features to the restricted IMU-kinematic feature set increased window-level accuracy from 87% to 90%, and the addition of IMU-kinematic data to the pressure sensors improved accuracy from 79% to 90%. Logistic regression (not in table) gave repetition-level accuracy comparable to random forest (88–100% vs. 92–100% across feature sets) but was consistently lower at the 3-s window level, especially for pressure-only features (e.g., elbow pressure: 47% vs. 62%). These comparisons indicate that pressure provided complementary information in this dataset, particularly when the IMU representation was limited; they do not establish that sensor fusion generally improves activity recognition.

Table 1: Activity classification accuracy by sensor feature set for random forest.

Feature Set	Classification Accuracy (%)	
	Repetition (n = 40)	3-s Window (n = 538)
IMU + pressure	**100%**	**99%**
IMU kinematics + pressure	**100%**	90%
Pressure (hand + elbow)	**100%**	79%
IMU kinematics (wrist + arm)	98%	87%
Wrist IMU only	92%	72%
Upper-arm IMU only	95%	73%
Hand pressure only	92%	69%
Elbow pressure only	**100%**	62%

Note. IMU kinematics excludes posture and duration features. Bold values indicate the highest accuracy in each column.

Distinguishing Stretching Conditions

The separate stretching recordings tested whether the sleeve signals distinguished instructed variations within one activity (Table 2). For full-range stretching versus the other conditions, combined IMU and pressure features achieved 100% repetition-level and 99% window-level accuracy. For four-way classification, the corresponding accuracies were 100% repetition-level and 99% window-level. IMU-only features performed similarly, while pressure-only features were less accurate for four-way classification, especially in three-second windows. Logistic regression matched random forest for the combined IMU+pressure feature set (98–100% across granularities and tasks) and showed no consistent advantage for either model on the single-sensor feature sets, unlike the activity-classification result. The classification results show that the recorded conditions had distinguishable signal patterns but do not demonstrate measurement of absolute range of motion or reliable recognition of prescribed range levels.

Table 2: Range-of-motion classification accuracy for stretching.

Feature Set	Binary (full vs. rest)		Four-way	
	Repetition	3-s Window	Repetition	3-s Window
IMU + pressure	**100%**	**99%**	**100%**	**99%**
IMU (both sensors)	**100%**	97%	**100%**	95%
Pressure (both sites)	90%	94%	82%	69%
Wrist IMU only	**100%**	89%	95%	77%
Upper-arm IMU only	95%	90%	90%	87%
Hand pressure only	90%	90%	55%	58%
Elbow pressure only	88%	67%	82%	38%

Note. Random forest with temporal cross-validation; n = 40 repetitions and 411 windows. Bold indicates the highest accuracy in each column.

Scope of the Proof of Concept

Together, these results show that the custom-fitted sleeve can record synchronized upper-limb motion and localized textile-sensor responses, and that these signals capture differences among the activities and stretching recordings examined here. The study includes one participant, with each activity and stretching condition associated with a particular recording. Consequently, recording-specific factors may contribute to the classification results, and performance on new participants, sessions, or garment placements remains unknown. The analyses were performed after acquisition and do not establish online classification latency.

LIMITATIONS AND FUTURE WORK

To build on this proof of concept, further work is needed to evaluate the robustness of the system across participants, repeated sessions, garment placements, and movement conditions. Future studies should also investigate calibrated pressure measurements, real-time processing, larger participant cohorts, and repeated-motion experiments to assess the consistency and reliability of the sensing approach and its potential applications in activity monitoring, rehabilitation, and adaptive smart garments.

CONCLUSION

This study demonstrates the feasibility of a fabric-based multimodal wearable system that integrates inertial and textile pressure sensing to capture both upper-limb motion and localized body–garment interactions. A key aspect of the approach is the use of a custom-fitted garment derived from an individual 3D body scan, enabling the sensing elements to be incorporated within a sleeve designed around the wearer's body geometry. This personalized fit provides a consistent interface between the body, garment, and embedded sensors, supporting the simultaneous measurement of movement and localized pressure responses. Across the activities examined, the synchronized sensor

signals revealed distinct combinations of movement and pressure response, while the classification experiments showed that pressure sensing can provide complementary information to IMU-based motion measurements, particularly for shorter analysis windows and restricted kinematic feature sets. The stretching experiments further demonstrated that the system could distinguish signal patterns associated with different instructed movement conditions. Together, these findings establish a proof of concept for a body-specific, multimodal textile sensing approach that combines customized garment design with integrated motion and pressure measurements for movement assessment.

REFERENCES

Abouraddy AF, Bayindir M, Benoit G, Hart SD, Kuriki K, Orf N, Shapira O, Sorin F, Temelkuran B, Fink Y. Towards multimaterial multifunctional fibres that see, hear, sense and communicate. Nature Materials 2007;6(5):336–347.

Angelucci A, Cavicchioli M, Cintorrino IA, Lauricella G, Rossi C, Strati S, Aliverti A. Smart textiles and sensorized garments for physiological monitoring: A review of available solutions and techniques. Sensors 2021;21(3):814.

Breiman L. Random Forests. Machine Learning 2001;45:5–32.

Castano LM, Flatau AB. Smart fabric sensors and e-textile technologies: A review. Smart Materials and Structures 2014;23(5):053001.

Cheng J, Sundholm M, Zhou B, Hirsch M, Lukowicz P. Smart-surface: Large scale textile pressure sensors arrays for activity recognition. Pervasive and Mobile Computing 2016;30:97–112.

Gravina R, Alinia P, Ghasemzadeh H, Fortino G. Multi-sensor fusion in body sensor networks: State-of-the-art and research challenges. Information Fusion 2017;35:68–80.

Homayounfar SZ, Andrew TL. Wearable sensors for monitoring human motion: A review on mechanisms, materials, and challenges. SLAS Technology 2020;25(1):9–24.

Iosa M, Picerno P, Paolucci S, Morone G. Wearable inertial sensors for human movement analysis. Expert Review of Medical Devices 2016;13(7):641–659.

Krogh A, Hertz JA. "A Simple Weight Decay Can Improve Generalization", proceedings of Advances in Neural Information Processing Systems 4 (NIPS 1991) (1991).

McCullagh P, Nelder JA. Generalized Linear Models, 2nd ed. London: Chapman and Hall (1989).

Moeslund TB, Hilton A, Krüger V. A survey of advances in vision-based human motion capture and analysis. Computer Vision and Image Understanding 2006;104(2–3):90–126.

Mokhlespour Esfahani MI, Nussbaum MA. Classifying diverse physical activities using "Smart Garments". Sensors 2019;19(14):3133.

Piao J, Kim M, Kim J, Kim C, Han S, Back I, Koh J-S, Koo S. Development of a comfort suit-type soft-wearable robot with flexible artificial muscles for walking assistance. Scientific Reports 2023;13(1):4869.

Porciuncula F, Roto AV, Kumar D, Davis I, Roy S, Walsh CJ, Awad LN. Wearable movement sensors for rehabilitation: A focused review of technological and clinical advances. PM&R 2018;10(9 Suppl 2):S220–S232.

Qiu S, Zhao H, Jiang N, et al. Multi-sensor information fusion based on machine learning for real applications in human activity recognition: State-of-the-art and research challenges. Information Fusion 2022;80:241–265.

Stoppa M, Chiolerio A. Wearable electronics and smart textiles: A critical review. Sensors 2014;14(7):11957–11992.
Xu G, Wan Q, Deng W, Guo T, Cheng J. Smart-Sleeve: A wearable textile pressure sensor array for human activity recognition. Sensors 2022;22(5):1702.
Zhang J, Zhang Y, Li Y, Wang P. Textile-based flexible pressure sensors: A review. Polymer Reviews 2022;62(1):65–94.
Zhao Y, Lv W, Xu S, Wei J, Wang G, Dang Q, Liu Y, Chen J. "DETRs Beat YOLOs on Real-time Object Detection", proceedings of IEEE/CVF Conference on Computer Vision and Pattern Recognition (CVPR), Seattle, Washington, pp. 16965–16974 (2024).